JOURNAL OF GEOPHYSICAL RESEARCH, VOL. 92, NO. C3, PAGES 2859–2874, MARCH 15, 1987

Comparison of Satellite-Derived Sea Surface Temperatures With in Situ Skin Measurements

P. SCHLUESSEL

Institut für Meereskunde, Kiel, Federal Republic of Germany

H.-Y. SHIN AND W. J. EMERY

Department of Oceanography, University of British Columbia, Vancouver, British Columbia, Canada

H. GRASSL

Forschungszentrum Geesthacht, Geesthacht, Federal Republic of Germany

Sea surface temperatures (SSTs), computed from sensor systems on the National Oceanographic and Atmospheric Administration (NOAA) polar-orbiting satellites, are compared with surface skin temperatures (from an infrared radiometer mounted on a ship) and subsurface temperature measurements. Three split window retrieval methods using channels 4 and 5 of the NOAA 7 advanced very high resolution radiometer (AVHRR) sensor were investigated. These methods were (1) using AVHRR alone, (2) using AVHRR with atmospheric temperature and water vapor profiles from the TIROS operational vertical sounder (TOVS), and (3) using AVHRR and data from the high-resolution infrared sounder (HIRS). TOVS sensors (including HIRS) are carried by the same satellite as the AVHRR and provide simultaneous corrections for the AVHRR-based SST estimates. The importance of scan angle correction to define the correct atmospheric path is discussed, and the improvement of SST retrievals using sensor combinations is demonstrated with satellite versus ship skin temperature mean differences ranging from 0.55° to 0.73°C for AVHRR alone, from −0.39° to 0.71°C for AVHRR plus TOVS, and from 0.22° to 0.33°C for AVHRR plus HIRS. The improved SST accuracy by AVHRR plus HIRS is due to additional correction for the atmospheric water vapor and temperature structures, made possible with some of the HIRS channels. Significant differences between ship skin and subsurface temperatures were observed, with the mean deviation being 0.2°C for a range of temperature differences between −0.25° and 0.6°C.

1. INTRODUCTION

Recently, the increased interest in climate change has led to a reappraisal of the measurement and mapping of sea surface temperature (SST). Historically, ocean surface temperatures were mapped from ship reports of bucket and later ship injection (engine room cooling water) temperatures. The need for surface temperature estimates from regions not often traversed by ships prompted the computation of ocean surface temperature from infrared satellite imagery. This application of satellite radiance data has undergone a steady evolution from an early operational product [*Brower et al.*, 1976] to a blend of satellite, ship, and buoy data (*Oceanographic Monthly Summary*, August 1984).

The primary problem in using infrared satellite imagery to estimate sea surface temperature is the presence of cloud and the attenuation of the ocean temperature signal by atmospheric water vapor. Correcting for atmospheric effects has led to a variety of new techniques, many of which have been intercompared in a series of workshops at the Jet Propulsion Laboratory (JPL) in Pasadena, California. Final results of this workshop series are reported in a number of articles in the November 1985 issue of the *Journal of Geophysical Research*.

A general conclusion of these workshops was that for the present set of satellite sensors the advanced very high resolution radiometer (AVHRR/2), flying on the National Oceanographic and Atmospheric Administration (NOAA) series of polar-orbiting satellites, leads to the best estimate of ocean surface temperature [*McClain et al.*, 1985; *Bernstein and Chelton*, 1985]. The most widely accepted atmospheric correction procedure is the multichannel sea surface temperature (MCSST) procedure introduced by *McClain* [1981]. As is further described by *McClain et al.* [1983] and compared with other approaches by *McClain et al.* [1985], the MCSST method is capable of producing surface temperatures accurate to within biases of 0.3°C and rms deviations of about 0.5°C. This correction procedure employs the different radiances in the two or three infrared channels of the AVHRR/2 system to remove the atmospheric water vapor contamination. The coefficients applied to the measured radiances in the two infrared channels are derived by the regression of computed sea surface temperatures on in situ measurements from ocean buoys. Verification of resulting accuracies are then made by comparison with an independent set of in situ surface temperature measurements.

All of the sea surface temperature calculation procedures used in the JPL workshops depended on comparisons with ship, buoy, and expendable bathythermograph (XBT) temperatures for either the specification (calculation of the regression coefficients) or the verification of the method. It is well known that the infrared satellite measurements really only apply to a very thin surface skin layer of the ocean [*Grassl*, 1976; *Paulson and Simpson*, 1981; *Robinson et al.*, 1984]. Thus all of the comparisons between infrared satellite measurements and ocean bulk temperatures are subject to deviations due to the differences between skin and bulk temperatures. In the following study we have examined a variety of atmospheric correc-

Paper number 6C0634.
0148-0227/87/006C-0634$05.00

TABLE 1. Regression Coefficients for Equation (3)

Scan Angle, deg	a_0, °C	a_1	a_2	Rms Error, °C
	Radiometric Plus Atmospheric Noise			
0	−0.99	3.659	−2.641	0.61
10	−1.01	3.688	−2.670	0.62
20	−1.05	3.774	−2.756	0.64
30	−1.14	3.918	−2.899	0.70
40	−1.21	3.926	−2.904	0.70
50	−1.53	4.207	−3.172	0.79
	Atmospheric Noise Only			
0	−1.23	4.000	−3.004	0.34
10	−1.25	4.027	−3.031	0.35
20	−1.29	4.089	−3.093	0.38
30	−1.37	3.206	−3.229	0.43
40	−1.46	4.230	−3.229	0.43
50	−1.83	4.500	−3.485	0.53

tion procedures for AVHRR data and have compared them with coincident infrared radiometer data (an actual skin temperature estimate) collected from ships in the eastern Atlantic and northeastern Pacific oceans. Also measured from the ships were in situ temperatures from thermistors below the ocean's surface. AVHRR radiances are atmospherically corrected by using other systems on the NOAA satellites to correct for water vapor contamination. Most successful is the correction of the AVHRR data using the high-resolution infrared sounder (HIRS) data.

We discuss first the theoretical aspects of the multispectral corrections. We then present results of radiative transfer simulations leading to the two instrument multispectral correction methods. Finally, some case studies of satellite- and ship-mounted radiometer measurements are presented in order to compare satellite-derived sea surface temperatures with in situ surface skin measurements.

2. SST Retrieval Procedures

In order to solve for the surface temperature in the radiative transfer equation (RTE), one must have accurate information on the temperature and the influencing gases composing the atmospheric profile in the field of view (FOV). It is very unlikely that this information will be routinely available, making it impractical in an operational environment to correct the surface temperature for complete atmospheric water vapor and temperature profiles. By viewing the same spot at two different path lengths, or at two wavelengths, one can efficiently estimate the above atmospheric effects. The method of using several infrared channels to correct for the atmospheric attenuation was suggested by *Anding and Kauth* [1970] and further developed by *McMillin* [1975], *McMillin and Crosby* [1984], and *Deschamps and Phulpin* [1983].

2.1. *Split Window Technique*

The split window technique (SWT) uses two neighboring atmospheric window channels for the correction. In the AVHRR/2 sensor these channels correspond to channels 4 (10.5–11.3 μm) and 5 (11.5–12.5 μm). The basis of the SWT is that a relationship exists between the surface temperature and the radiances measured by the two window channels. This assumption has been verified by several investigators [*Anding and Kauth*, 1970; *Deschamps and Phulpin*, 1983; *Prabhakara et al.*, 1974; *Ulivieri*, 1984].

The derivation of the SWT is well described in the above literature. The result of the derivation gives

$$B(\nu_1, T_s) = I_1 + \frac{(1-\tau_1)}{c(1-\tau_2)-(1-\tau_1)}(I_1 - I_2') \qquad (1)$$

where I_i is the observed radiance and τ_i is the atmospheric transmittance at wavelength ν_i. If the Planck's function $B(\nu_1, T_s)$ is inverted, the surface temperature T_s can be obtained. The coefficient of the correction term is a strong function of water vapor content. Thus *Dalu et al.* [1981] found that if an independent means of estimating water vapor content is available, the SST measurement can be improved. *McMillin and Crosby* [1984] provided an alternate method directly involving brightness temperature values. If a Taylor expansion to the Planck's function about the temperature is used, the following SWT algorithm can be derived:

$$T_s = T_1 + \gamma(T_1 - T_2) + \delta \qquad (2)$$

The values for γ and δ can be obtained from a sample of atmospheres, or it can be found by performing a regression against in situ measurements.

In order to study the impact of atmospheric water vapor and temperature structures, together with the scan angle variation of the radiometer, on the radiance measured in the AVHRR/2 split window, radiative transfer calculations have been performed for a set of 182 tropical and mid-latitude atmospheres accounting for seasonal variations. Computed brightness temperatures of AVHRR channels 4 and 5 are then used to fit the simulated surface skin temperatures by using a linear regression model to find a set of coefficients for the split window formula

$$T_s = a_0 + a_1 T_4^A + a_2 T_5^A \qquad (3)$$

where T_i^A represents the brightness temperatures in the split window channels (for more details see *Strong and McClain* [1984]) and T_s represents the sea surface temperature. The sea surface skin temperatures were simulated by assuming that the skin temperatures were normally distributed about the surface air temperature with a standard deviation of 2.5°K. A noise level of 0.12°K in the brightness temperatures was considered within the simulations to account for radiometric noise. A wide variety of atmospheric situations were included in the same regression to retrieve the quasi-global set of coefficients a_i given in Table 1.

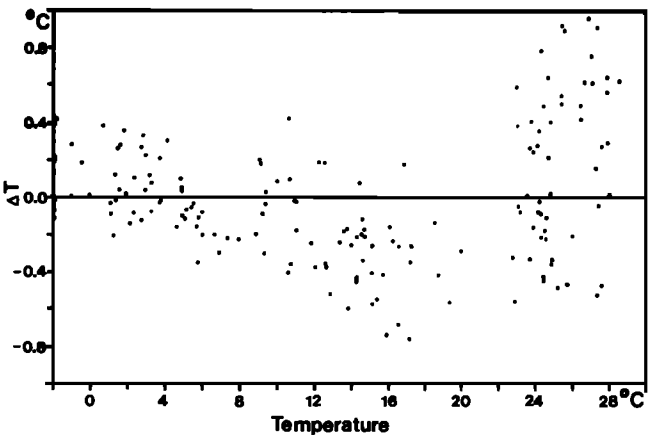

Fig. 1. Differences between real surface skin temperature and the satellite temperature retrieved from the regression (atmospheric plus radiometric noise) for nadir view using the coefficients in Table 1 over real surface skin temperature.

The numbers in Table 1 demonstrate the strong scan angle dependency, with increasing standard errors at larger scan angles, indicating the impact of atmospheric structure on the radiances seen at the satellite altitude. The importance of scan angle correction for the calculation of sea surface temperature from multichannel AVHRR data has recently been emphasized by *Barton* [1985] and *Kelly and Davis* [1986]. Other studies [*Maul*, 1983; *Dalu*, 1985] have also investigated the magnitude of SST errors due to differences in scan angle. However, in part owing to the explicit use of the scan angle, the simulation rms errors in Table 1 are slightly smaller than those found by *Strong and McClain* [1984] and *Strong* [1984] for satellite and drifting buoy match-ups. The retrieval coefficients seem more robust against atmospheric peculiarities whose impacts increase at larger scan angles. A further study of the numerical simulation was done by comparing the observed surface skin temperatures with those computed from the synthetic brightness temperatures using (3). Figure 1 shows the differences between these two SSTs plotted against the measured surface skin temperature, giving a first impression about systematic errors introduced when using a simple two-channel approach. Since these errors increase with increasing scan angle, they must be caused by variations in the atmospheric structure.

Similar work was done by *Llewellyn-Jones et al.* [1984], who derived regionally dependent coefficients for the North Atlantic and for the tropical oceans. In order to test our radiation transfer model, the coefficients have been applied to calculate synthetic brightness temperatures for nadir views for comparison with the original surface temperatures. Because of the regional dependency, the data set was split into two subsets, tropical (53 cases) and mid-latitude (129 cases) regions. The retrieved surface temperatures showed similar scatter around the true surface values as in our own regression: 0.50°K standard deviation for the mid-latitude atmospheres and 0.77°K in the tropics. More important, the biases were almost negligible: $T_s - T_s^L = 0.11$°K in middle latitudes and $T_s - T_s^L = 0.03$°K in tropical situations (T_s^L is the surface temperature predicted by *Llewellyn-Jones et al.* [1984]). These results confirmed the validity of the radiative transfer simulations. By performing the same test with *McClain et al.*'s [1985] coefficients, covering all scan angles and several atmospheric/oceanic situations, a standard deviation of 0.97°K was observed from 1092 samples. The bias was −0.34°K, which was expected and which demonstrated the spread between

TABLE 2. Regression Coefficients for Equation (7)

Scan Angle, deg	a_0, °C	a_1	a_2	a_3	a_4	Rms Error, °C
			Radiometric Plus Atmospheric Noise			
0	13.27	3.239	−2.261	0.0734	−7.021	0.54
10	13.52	3.271	−2.295	0.0762	−7.131	0.55
20	13.84	3.388	−2.419	0.0849	−7.240	0.56
30	14.55	3.591	−2.633	0.1010	−7.500	0.61
40	13.38	3.653	−2.688	0.0967	−6.882	0.62
50	11.74	4.118	−3.154	0.1130	−5.921	0.72
			Atmospheric Noise Only			
0	3.59	4.442	−3.537	0.119	−1.752	0.20
10	3.76	4.471	−3.568	0.121	−1.819	0.20
20	3.91	4.554	−3.657	0.128	−1.838	0.22
30	4.15	4.725	−3.839	0.144	−1.838	0.26
40	2.81	4.781	−3.883	0.132	−1.194	0.27
50	0.65	5.191	−4.288	0.142	−0.0416	0.35

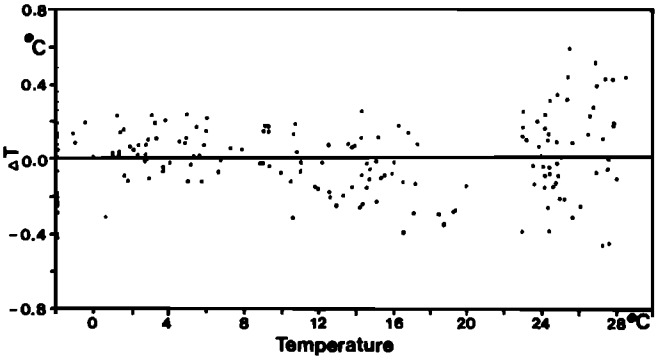

Fig. 2. Same as in Figure 1 but for coefficients from Table 2.

skin and bulk surface temperatures. Since McClain's coefficients are retrieved by regression between in situ bulk temperatures and AVHRR measurements, simulations were designed to give skin temperatures which were normally 0.1°–0.5°K cooler than temperatures at a depth of around 1 m [*Robinson et al.*, 1984].

An examination of those cases with the largest differences between measured and satellite-retrieved surface skin temperatures points to two different sources of the large errors in the split window results. First, for $T_{air} > T_s$, which is a standard condition in coastal waters in spring, the brightness temepratures predict far higher SST values than really occur. Second, extremes of water vapor content in the atmosphere (e.g., tropical atmospheres with especially high water vapor contents or "dry lines" just behind cold front passages showing considerably drier conditions than "normal" atmospheres) require atmospheric corrections that lie beyond the range of the split window coefficients. Consequently, an improvement of the split window SST retrievals should be possible with additional information about the low-level tropospheric temperature structure and the water vapor anomalies at heights that are not covered by the AVHRR window channel atmospheric weighting functions.

2.2. *AVHRR and TIROS Operational Vertical Sounder Combined Methods*

One possibility to overcome the difficulties which arise with the simple split window approach (which suffers from a poor knowledge of the thermodynamic state of the atmosphere) is to use atmospheric sounder data from other radiometers on board the same satellite. The TIROS operational vertical sounder (TOVS) package with its HIRS and microwave sounding unit may be able to deliver adequate information to correct the systematic errors in the split window SST retrievals caused by the atmosphere. However, the assumption of horizontal homogeneity of atmospheric temperature and moisture fields within one sounder resolution element has yet to be justified.

TABLE 3. Information About NOAA 7 Orbits Used

Orbit	Node	Date	Time, UT	Latitude, °N	Longitude, °W
17667	ascending	Nov. 25, 1984	1622	46.29	8.61
				48.47	5.37
17681	ascending	Nov. 26, 1984	1607	37.62	9.91
				51.24	15.34
15779	ascending	July 14, 1984	2359	48.07	125.60
				48.66	125.13

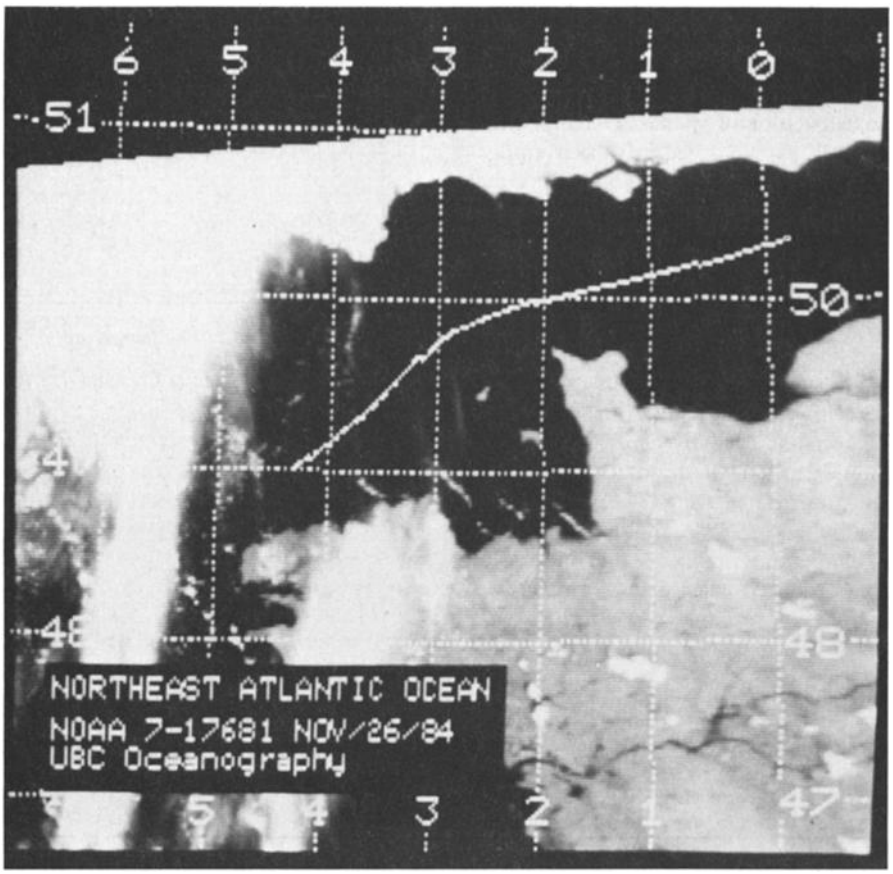

Fig. 3*a*

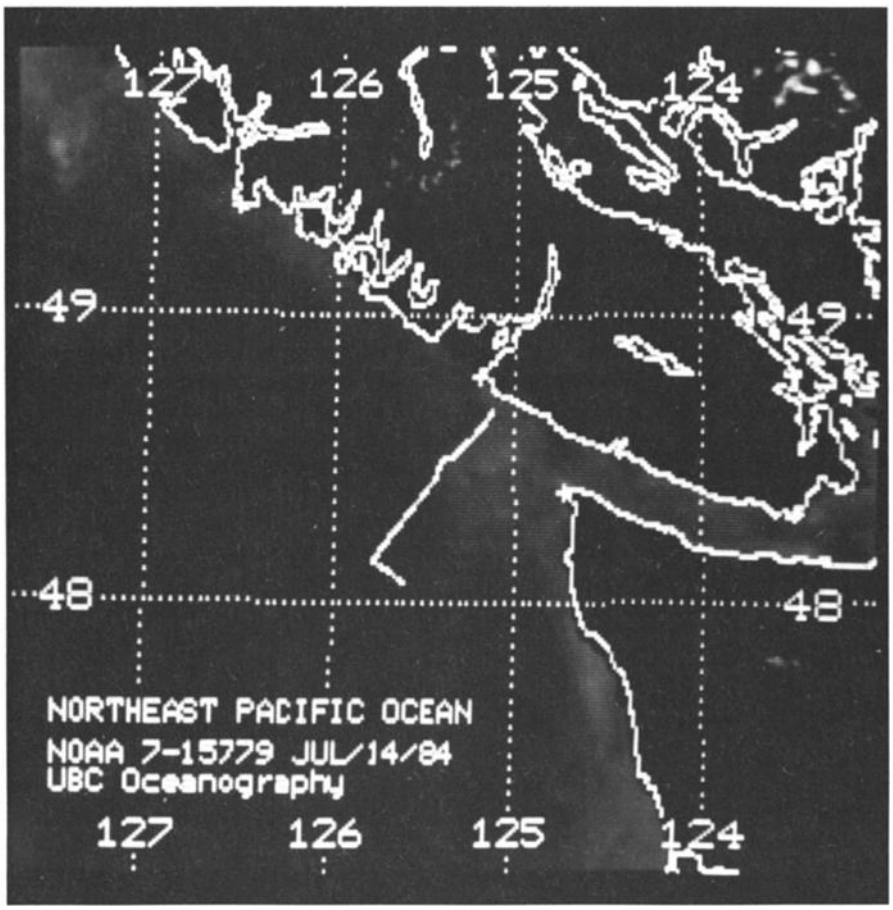

Fig. 3*b*

Fig. 3. NOAA AVHRR channel 4 imagery for orbit numbers (*a*) N7-17681 and (*b*) N7-15779.

Generally, two different methods can be applied to improve the accuracy of satellite-borne SSTs by using a coupled AVHRR/TOVS system. One way is to retrieve TOVS temperature and moisture profiles, which then provide the exact transmission functions for the atmosphere and hence give a refinement of the split window retrieval coefficients. Another method is to extend the split window approach, with HIRS channels, accounting in a statistical way for atmospheric variability. For both methods the main disadvantage is the difference in the FOV of AVHRR and TOVS systems. The coarse-resolution elements of the TOVS sounder must be interpolated to the AVHRR scan patterns, making the SST retrievals partly subject to the interpolation method used.

2.2.1. *AVHRR retrieved SST using TOVS-derived profiles.* The first SST correction method uses TOVS profiles computed from the physical process of solving the radiative transfer equations for the atmosphere; this method does not require any external surface observations and is thus most attractive. Keeping in mind the emittance effect (increase in apparent SST due to downwelling atmospheric radiance), the success of this SST correction method depends on the capability of the TOVS sensors, the accuracy of the profile retrieval technique, and the correctness of the transmission model for the interacting atmospheric gases. The capability of TOVS to supplement radiosonde (RAOB) data where observation stations are sparse has been shown by *Kelly et al.* [1983]. The comparison of TOVS retrieved temperature and moisture profiles with radiosonde data has been performed by *Philips et al.* [1979], *Bruce et al.* [1977], *Hillger and Vonder Haar* [1979], *Moyer et al.* [1978], and *Hayden et al.* [1981]. Even though the two measurements were over the same atmosphere, the measured characteristics differed significantly. Radiosondes make point measurements as they continuously ascend, whereas TOVS makes horizontally and vertically integrated measurements. The rms statistics between these two different measurements do not provide proper accuracy estimates of the TOVS retrievals. Such comparisons are, however, the only available way to gain some confidence in the TOVS retrievals. The moisture profiles produced even poorer results, with the dew point rms deviations as large as 7.3°C. However, *Moyer et al.* [1978] reported that when moisture profiles were analyzed in terms of total integrated precipitable water, the deviation was only 20% of the total precipitable water.

TOVS sounding of the atmosphere involves retrieving vertical profiles of temperature and moisture from a number of discrete radiance measurements. For the HIRS/2 infrared sounder on board the NOAA spacecraft, there are eight channels near 15 μm and five channels near 4.3 μm in the CO_2 absorption bands of the infrared spectrum to derive temperature profiles. The radiances to estimate atmospheric moisture are measured with three channels near the 6.7-μm band of the water vapor absorption spectrum.

Because only a finite number of measurements are available, the problem of inverting the nonlinear RTE to solve for the surface radiance is ill posed; i.e., there are a number of possible solutions. In order to converge on a single solution, additional external constraints are necessary. The additional constraints can be obtainced from independent atmospheric profiles, such as those from radiosondes. This approach is usually fast, and convergence is always achievable. However, the involvement of statistics limits the validity to local regions where the RAOB samples are taken. The requirement for up-to-date RAOB data, for example, over an open ocean, imposes a practical limitation to the method. Also, it is possible that a solution that represents the true state of the atmosphere (perhaps a strong anomaly) may be rejected because the general statistical constraints for typical atmospheric structures do not allow it.

An alternate to the indirect, statistical approach is to directly solve the RTE using an iterative procedure. This method has the disadvantage of requiring a representative initial profile, and convergence is not always guaranteed. Also, there is no way of knowing to which solution the process has converged. The iterative process used to retrieve the temperature profile is from *Smith et al.* [1983] and is as follows:

$$T^{n+1}(p) = T^n(p) + \frac{\sum_{i=1}^{m}[T_B(\nu_i) - T_B{}^n(\nu_i)]W^n(\nu_i, p)}{\sum_{i=1}^{m}W^n(\nu_i, p)} \tag{4}$$

where $T^n(p)$ is the nth iteration temperature at pressure p, m is the number of channels, $T_B{}^n$ is the brightness temperature calculated from the temperature profile $T^n(p)$, and the weighting function is

$$W^n(\nu_i, p) = \frac{B[\nu_i, T^n(p)]d\tau^n(\nu_i, p)}{R^n(\nu_i)\,dp}$$

$R^n(\nu_i)$ is the nth iteration Planck's radiance for channel ν_i emerging at the top of the atmosphere. The iteration is terminated when the brightness temperature difference between two successive iterations is less than 0.05°C.

The iteration procedure for the moisture profile is from *Hillger* [1984]. This method is a variation of *Chahine*'s [1972, 1977] relaxation method to handle the temperature inversion near the surface that often exists over coastal areas of the ocean in the summertime. The moisture profile is expressed in terms of the mixing ratio, $Q(p)$. The iteration procedure is expressed as

$$Q^{n+1}(p) = Q^n(p)\left[1 - \frac{\sum_{i=1}^{3}S_i{}^n\Delta L_i{}^n\Delta\tau_i{}^n(p)}{\sum_{i=1}^{3}\Delta\tau_i{}^n(p)}\right] \tag{5}$$

where $\Delta\tau_i(p) = \tau_i(p_m) - \tau_i(p_{m+1})$, $\Delta L_i{}^n = L_{i,\text{obs}} - L_{i,\text{calc}}{}^n$, and S is the factor for converting from radiance change to mixing ratio change.

The atmospheric transmission for all HIRS IR channels is calculated by using the method described by *Weinreb et al.* [1981]. This method calculates transmittances for (1) spectral lines of the uniformly mixed gases (CO_2, N_2O, CH_4, CO, and O_2), (2) spectral lines of water vapor, (3) spectral lines of ozone, (4) the water vapor self-broadened continuum (dimer interaction), (5) the water vapor N_2-broadened continuum

TABLE 4. Thresholds Used to Detect Cloud Contamination

Orbit	Percent albedo$_1$	Percent albedo$_2$	T_5, °C
17667	>0.7	−0.8	<8.0
17681	>0.7	−0.8	<8.0
15779	>3.19	−1.65	<8.0

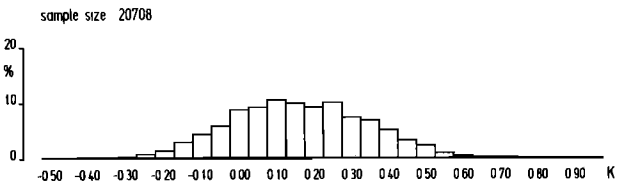

Fig. 4. Distribution of the differences between bulk water temperature, at a depth of 4 m, and surface skin temperature during the cruise of R/V *Meteor*, October/November 1984.

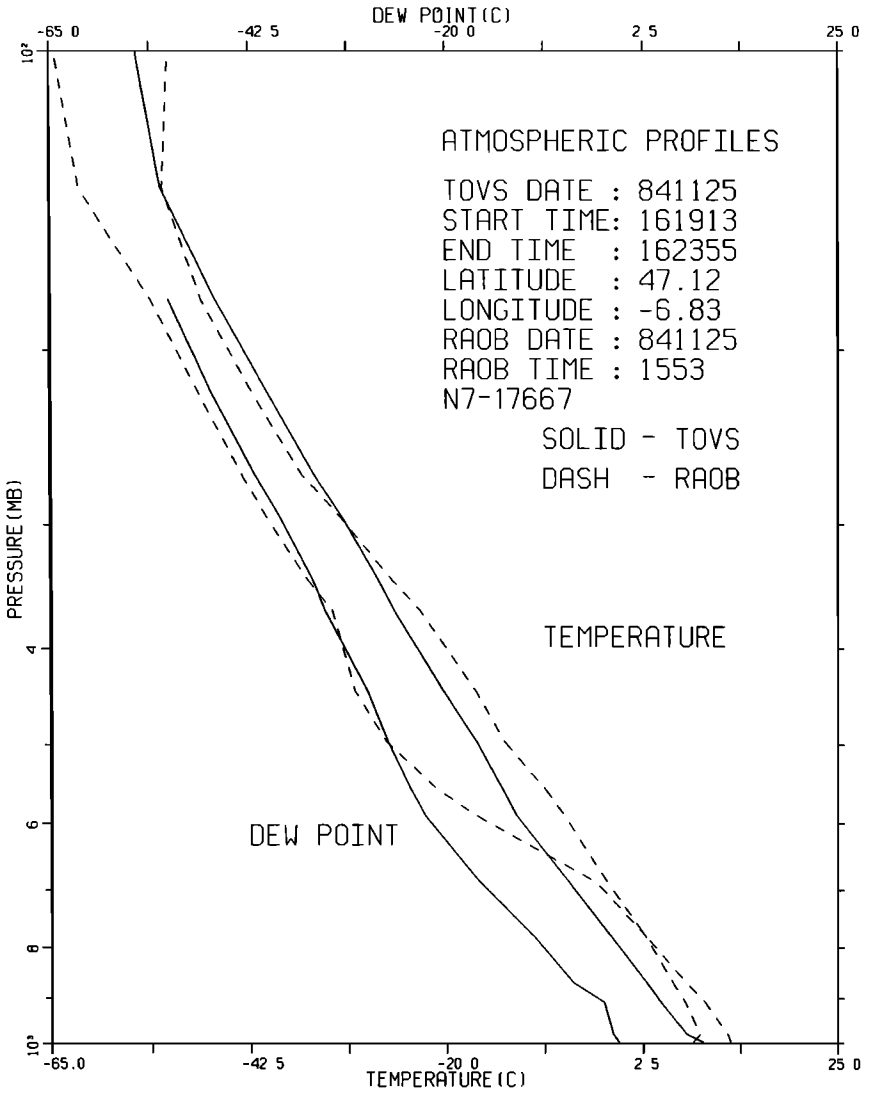

Fig. 5a

Fig. 5. Vertical atmospheric profiles from TOVS and RAOB for (*a*) November 25, 1984, (*b*) November 26, 1984, and (*c*) July 14, 1984.

(H_2O-N_2 interaction), and (6) the collision-induced band of molecular nitrogen.

The iterative scheme for solving the RTE requires initial temperature and moisture profiles. The climatological mean profiles for the latitude zone are used as the initial temperature profile. Unlike temperature, atmospheric moisture is highly variable, and the climatological mean moisture profiles do not make good initial guess profiles. The initial moisture profile is estimated from the surface temperature with lapse rates at several atmospheric levels estimated from the three HIRS water vapor channels. The surface temperature during the iterative process is estimated from the three HIRS/2 window channels.

2.2.2. *Extension of the AVHRR split window technique using HIRS.* The information needed for an adequate SST retrieval, even in pathological cases, can be taken from the HIRS channels that mainly monitor the atmosphere rather than the surface. The HIRS water vapor channel 11 has the maximum of its weighting function at approximately 700 mbars and therefore indicates properties of the vertical water vapor structure not detected by the AVHRR window channels. The use of this additional channel promises a supplemental correction in cases with extreme water vapor contents (abnormally dry or wet atmospheres).

HIRS CO_2 channels 6, 7, and 8 with weighting functions peaking at 700 and 900 mbars and at the surface, respectively, provide information about the temperature structure in the lower troposphere. The ratio

$$r = \frac{(T_8^H - T_6^H)}{(T_8^H - T_7^H)} \tag{6}$$

where T_i^H is brightness temperature in HIRS channel i, increases with atmospheric stability in lower tropospheric levels. One can expect for cases of extreme $(T_{air} - T_s)$ differences that the HIRS channels will provide a way to correct the AVHRR SST retrievals for these anomalous conditions. Hence an appropriate model is

$$T_s = a_0 + a_1 T_4^A + a_2 T_5^A + a_3 T_{11}^H + a_4 r \tag{7}$$

where T_i^A is the brightness temperature for AVHRR channel i. Computer simulations of the atmospheric radiative transfer

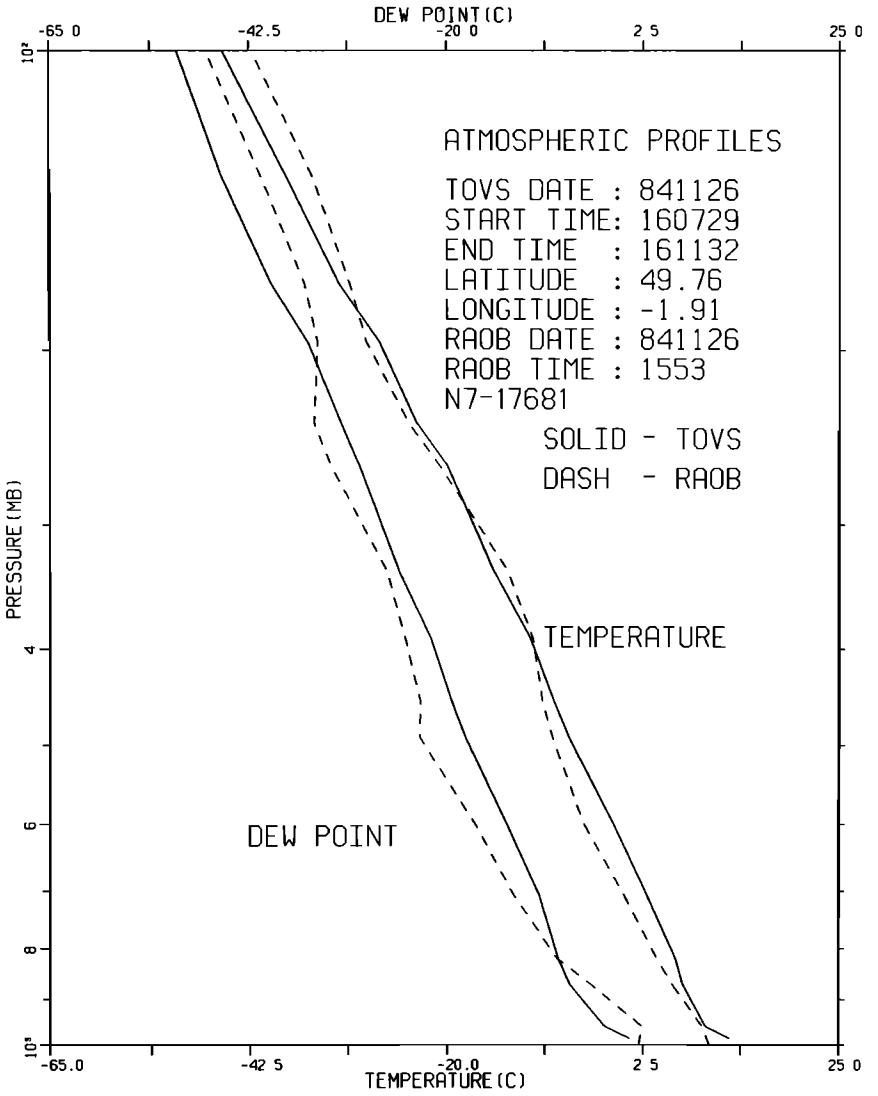

Fig. 5b

for the desired NOAA 7 channels have been performed for the above mentioned set of 182 atmospheres. The synthetic brightness temperatures are then fitted to (7) in order to regress the coefficients a_i given in Table 2. The radiometric noise again enters the radiative transfer calculations, leading together with the atmospheric errors, to the given rms values.

A comparison with Table 1 shows decreased temperature errors for all scan angles. Figure 2 includes, as does Figure 1, differences between true and regression temperatures. Figure 2 clearly demonstrates the elimination of extreme outliers and hence the potential of the extended split window method to give adequate results even for "complex" atmospheres. For example, the standard errors decreased from 0.34°C to 0.20°C at nadir view and from 0.53°C to 0.35°C at a scan angle of 50° in going from a stand-alone AVHRR retrieval to an AVHRR plus HIRS method. The lower halves of Tables 1 and 2 give coefficients and errors for a regression neglecting the radiometer noise, which can be achieved in practice by spatial averaging of the brightness temperatures over many pixels (about 100 are necessary). The remaining errors are due mainly to "atmospheric noise," which is systematic and cannot be reduced by spatial averaging.

3. Data Collection and Processing

3.1. *In Situ Measurements*

For a verification of the satellite SST retrieval methods, comparisons with in situ sea surface temperatures measured from ships or buoys are necessary. In most satellite SST verification studies [*McClain et al.*, 1985; *Bernstein and Chelton*, 1985], surface bucket, ship injection (engine cooling water), drifting buoy, and XBT surface temperatures have been used as measures of in situ SST. As has been mentioned earlier, there can be a significant difference between these "bulk" measures of SST and the skin temperature measured by the satellite radiometer. In order to better verify satellite skin temperature and be able to estimate the differences between this surface skin value and that of a meter or two down in the water column, two different field experiments were carried out. In the observations from both the North Atlantic and the eastern North Pacific, a ship-mounted radiometer continuously monitored surface skin temperature, while thermistors in the upper few meters measured the near-surface bulk temperature.

3.1.1. *North Atlantic Ocean.* On the cruise of R/V

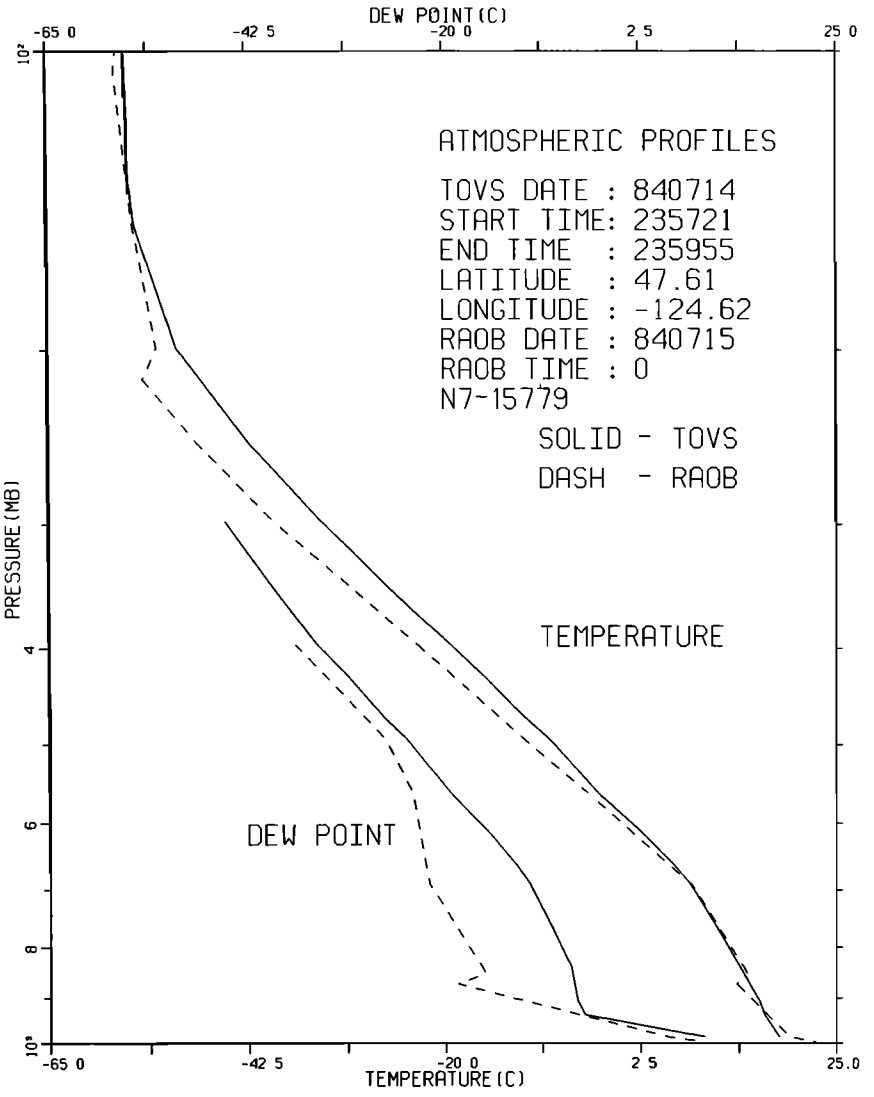

Fig. 5c

Meteor, from October 20 to November 28, 1984, temperature and radiation measurements were collected in the northeast Atlantic Ocean between latitudes 21°N and 54°N. Radiometric surface skin temperatures and water temperatures, at depths of 2, 4, and 7 m, were monitored continuously. The skin temperature was measured with a precision radiometer (Barnes PRT5 with an 8- to 14-μm band-pass filter) every 2 min as 1-min means. Every other minute was used for a calibration of the radiometer. The absolute accuracy of the skin temperature was calibrated to 0.05°C, which included the corrections for (1) the nonblackness of the sea surface at the measured spectral region, (2) the temperature drift of the internal reference target of the radiometer, (3) varying reflected radiation from clear sky, clouds, and the ship in the measured spectral region, and (4) instrumental noise limiting the resolution of the radiometer as outlined by *Grassl and Hinspeter* [1975]. The in situ water temperatures were sensed with platinum resistance thermometers (PT200) mounted at the specified depths and measuring 1-min temperature means with an accuracy of 0.0125°C. In order to match the shipborne temperatures with those measured by the satellite, the ship temperatures were time averaged. Since the ship's speed was about 11 knots (20 km/h), an averaging over 5 min seemed reasonable to match the FOV of a single AVHRR pixel. RAOBs were collected four times daily during the *Meteor* cruise in the Atlantic.

3.1.2. *North Pacific measurements.* Similar to the North Atlantic measurements, during the period of July 10 to July 19, 1984, the research vessel *Pandora II* was employed to collect both skin and bulk surface temperature measurements

TABLE 5. Results of Satellite-Ship Temperature Comparison

		AVHRR Alone		AVHRR Plus TOVS		AVHRR Plus HIRS	
Orbit	Sample Size	Bias	Standard Deviation	Bias	Standard Deviation	Bias	Standard Deviation
17667	78	0.01	0.78				
17681	158	0.55	0.31	−0.39	0.24	0.22	0.32
15779	204	0.73	0.51	0.71	0.36	0.33	0.45

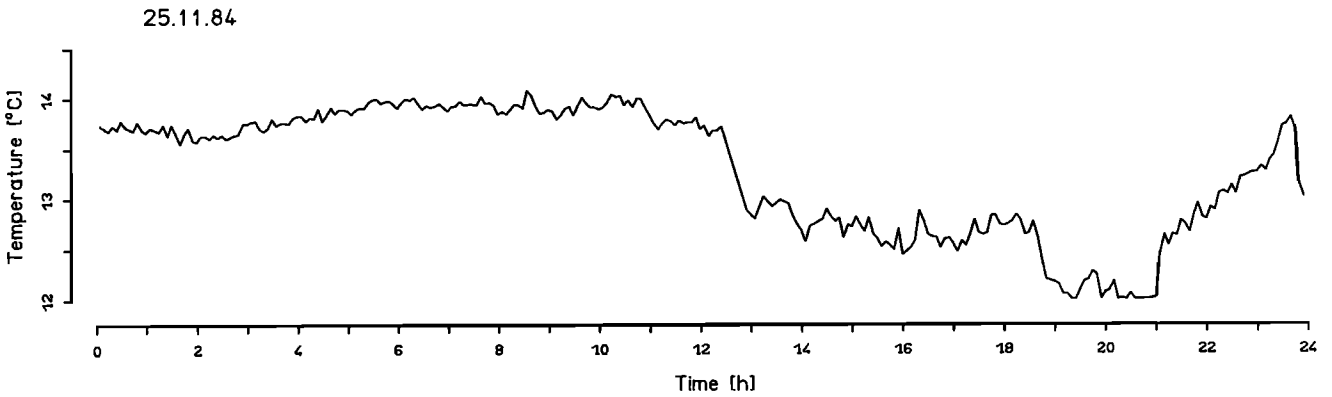

Fig. 6*a*. Time series of surface skin temperature along the track of R/V *Meteor* on November 25, 1984 (5-min means).

in the eastern North Pacific Ocean. The cruise area was to the west of Vancouver Island near 49°N and 125°W. The cruise tracks covered from Juan de Fuca Strait to Barclay Sound and extended out to the continental shelf break about 200 km offshore. Sea surface radiation was measured using a Barnes PRT5 radiometer sensing radiation for wavelengths from 9.5 μm to 11 μm in the infrared spectrum. The radiation averaged measurements were recorded at 2-min intervals. Unlike the Atlantic data, bias correction for the Pacific data was performed every 30 min. Calibration was done by mounting the radiometer facing a well-stirred water bath and measuring the surface radiation along with the temperature while the temperature of the water bath was varied from 0°C to about 25°C. The temperature of the water bath was recorded using a precision thermometer. RAOB data were not collected from the ship during the northeast Pacific cruise; instead, RAOB data from the nearest land station (Quillayute, Wash.) were used to validate TOVS-derived atmospheric profiles.

3.2. *Satellite Measurements*

Three different multichannel retrieval techniques, yet to be described, were applied to AVHRR/2 and TOVS data from the NOAA 7 spacecraft to compute SST. Three satellite passes, each matching a day of a ship's cruise, were examined for a comparison with the in situ measurements (Table 3). However, before the SST retrievals were performed, the satellite images were navigated and checked for cloud contamination. The channel 4 (11 μm) infrared AVHRR images for two of the three passes are shown in Figure 3*a* and 3*b*; these satellite images have added to them the corresponding ship tracks for the northeast Atlantic and northeast Pacific, respectively.

The satellite image navigation was done in two steps: modeling of the orbital mechanics of the spacecraft's orbit and the scan geometry of the radiometers provided a first guess of the geographic coordinates. Then further refinement was achieved by fitting high-resolution coastal lines to the image data, making the navigation accurate to within a pixel. The method is best suited for nadir viewing, giving a precision of about 1 km in the geographic registration of the image. The sounder with its coarser spatial resolution (17 km for a HIRS spot at nadir) can easily be matched to the image data, since the scan geometries of the radiometers and orbital elements of the spacecraft are known [*Aoki*, 1980]. After navigation and cloud check, the HIRS field is simply interpolated to the AVHRR field, using for each AVHRR location a distance-weighted mean of surrounding spots. The retrieval of AVHRR and HIRS radiance values over the ship's cruise track was accomplished by calculating the scan line and the pixel number for each sampled ship location and performing the weighted averaging over four adjacent pixels.

An important problem is the cloud detection for the AVHRR/2 on a single-pixel basis. For the methods that were described in sections 2.2.1 and 2.2.2, no "declouding" (i.e., computing of clear radiances from partially cloudy pixels) is attempted. If a pixel/spot is detected as being cloudy, it is rejected and no longer used. The cloud detection scheme used visible and infrared thresholds that were determined from histograms of all radiances within the area of interest [*Olesen and Grassl*, 1985; *Saunders*, 1985]. Thresholds chosen for each of the NOAA 7 passes are shown in Table 4.

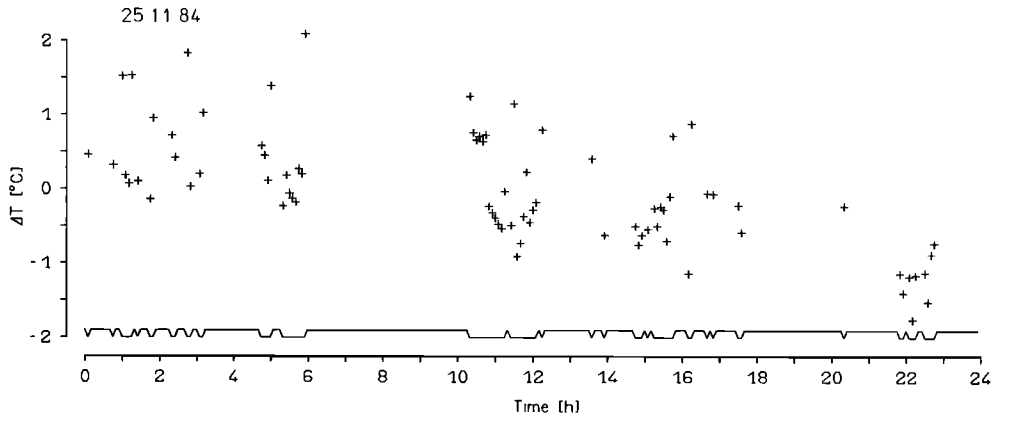

Fig. 6*b*. Differences between AVHRR-only retrieved skin temperatures and PRT5 measured ones; cloudy measurements are marked by the line at bottom of graph, and corresponding differences are set to zero.

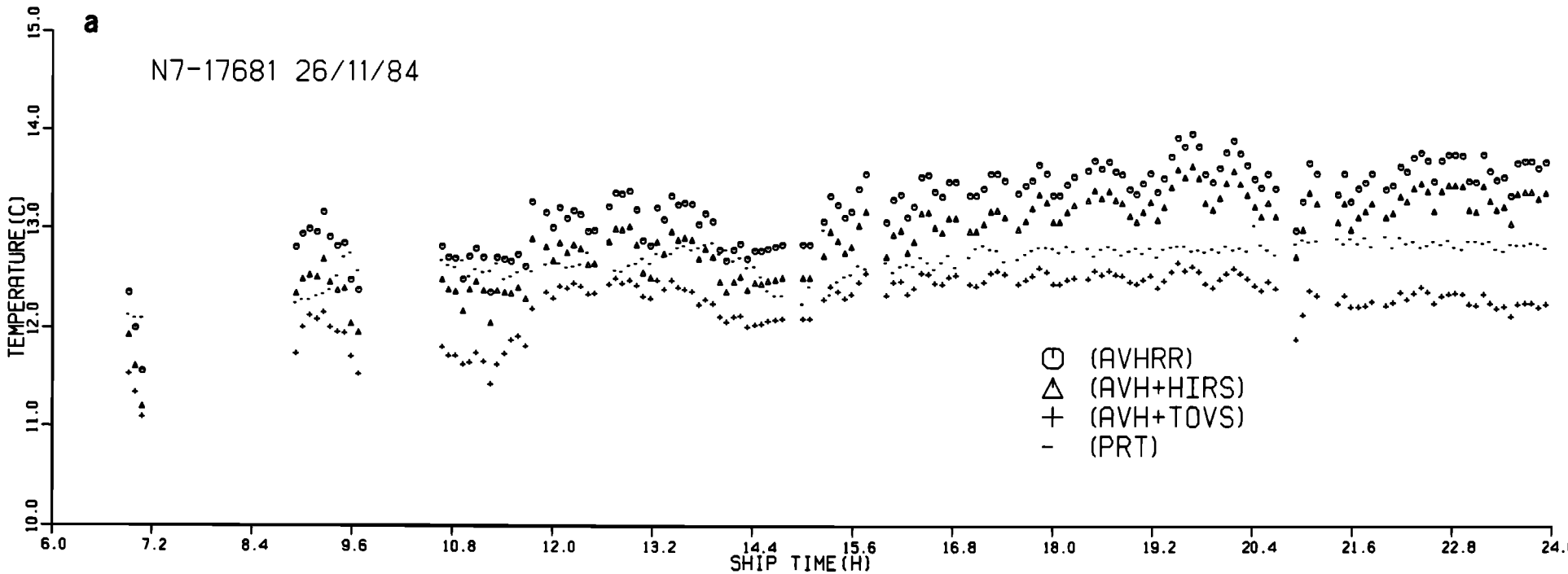

Fig. 7*a*. Time series of surface skin temperature along the track of R/V *Meteor* on November 26, 1984 (5-min means).

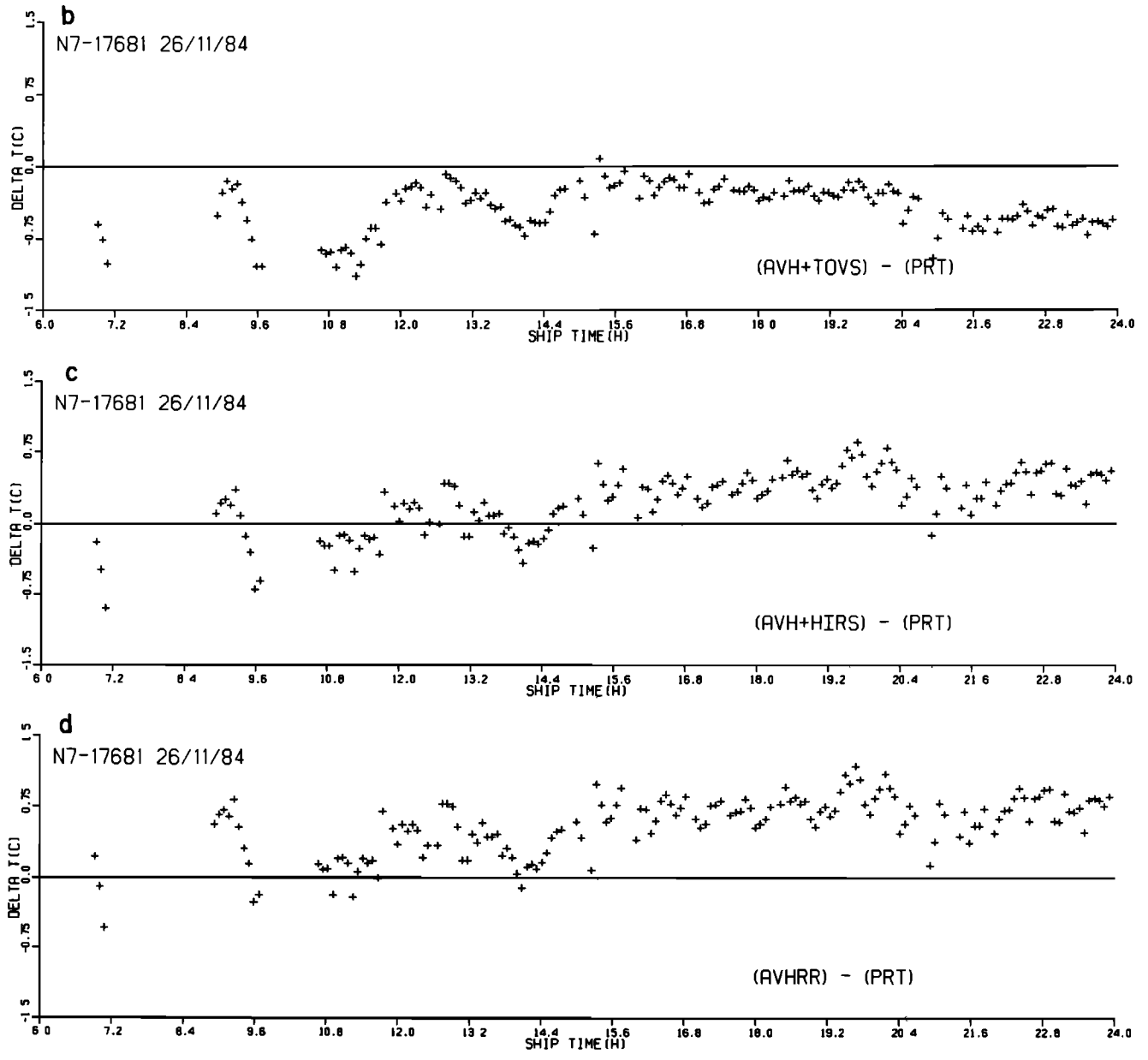

Fig. 7. (continued) Differences between PRT5 measured skin temperatures and (*b*) AVHRR plus TOVS retrieved skin temperatures, (*c*) AVHRR plus HIRS retrieved skin temperatures, and (*d*) AVHRR-only retrieved skin temperatures.

4. Relation of Surface Skin Temperature to Bulk Water Temperature

The ocean surface as seen by a radiometer usually has a cool skin, being approximately 0.1°–0.5°K colder than the water below [*Saunders*, 1967; *McAlister and McLeish*, 1969; *Hasse*, 1971; *Grassl and Hinzpeter*, 1975; *Grassl*, 1976, 1977; *Robinson et al.*, 1984]. This has to be kept in mind when comparing remotely sensed surface temperatures with ship-borne measurements. The skin temperature is balanced by the total heat flux at the ocean-air interface. Thereby the fastest response of the skin temperature is to variations in the net long-wave radiative flux, which establishes a balance between the surface emitted thermal radiation and the downwelling atmospheric radiation (which affects only the uppermost 10 μm of the ocean), followed by evaporative cooling in the viscous sublayer [*Grassl*, 1977]. This surface layer will be destroyed by the white capping of wind-induced waves at wind velocities above about 10 m/s [*Clauss et al.*, 1970]. This mixes the upper layer, resulting in smaller differences between skin and bulk water temperatures. For a strongly stratified upper ocean the diurnal heating, by incoming solar radiation, of the upper few centimeters will raise the near-surface temperatures, increasing the skin temperature. The result will be a surface skin that is warmer than the water at a depth of several meters. Hence the range of the surface skin temperature will be between some tenths of a degree or more higher than the bulk temperature and several tenths below it. Figure 4 shows a histogram of the bulk-skin temperature differences which occurred during the entire *Meteor* cruise. The 0.2°K mean deviation of the cool sea surface skin from the deeper in situ temperatures still leaves a range of values from −0.5°K to 0.9°K. Taking this fact into account, one may expect systematic uncertainties when comparing remotely sensed SSTs to bulk temperatures that lie in the range of the SST accuracy required (0.3°C) for climate applications.

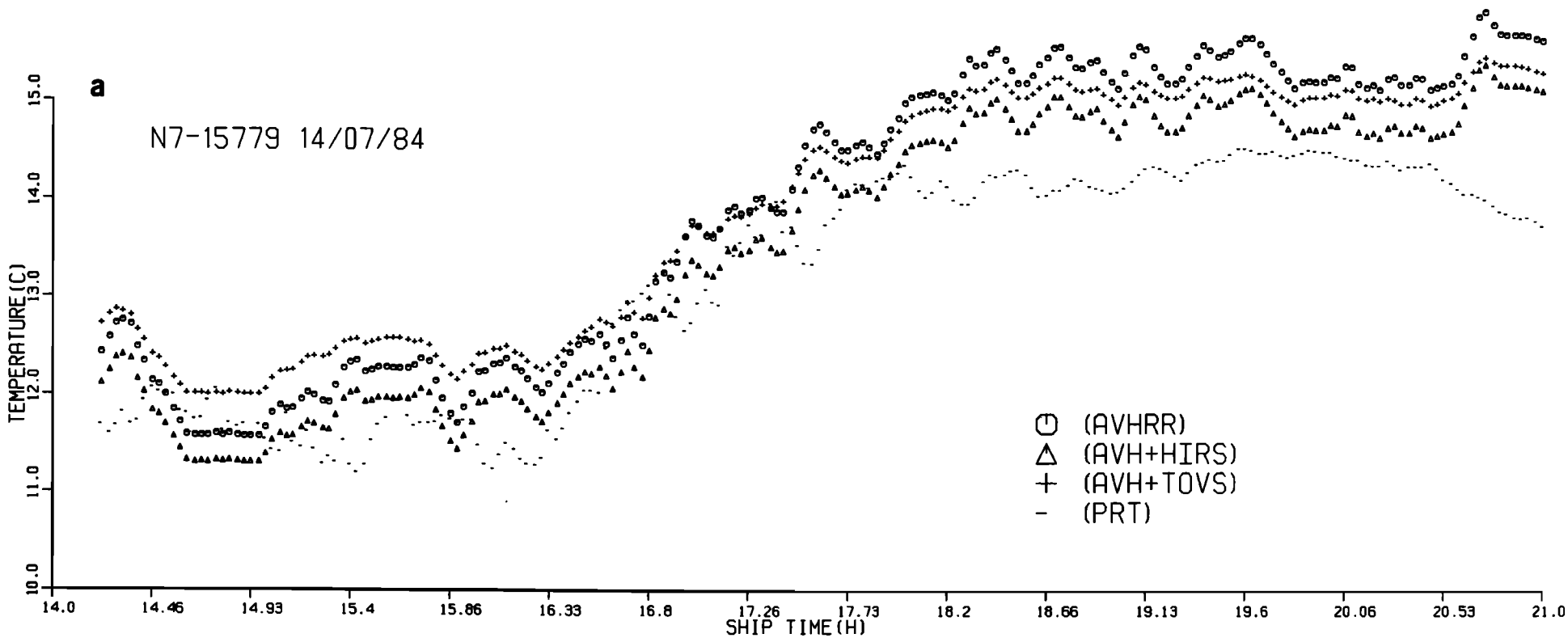

Fig. 8*a*. Time series of surface skin temperature along the track of *Pandora II* on July 14, 1984 (2-min means).

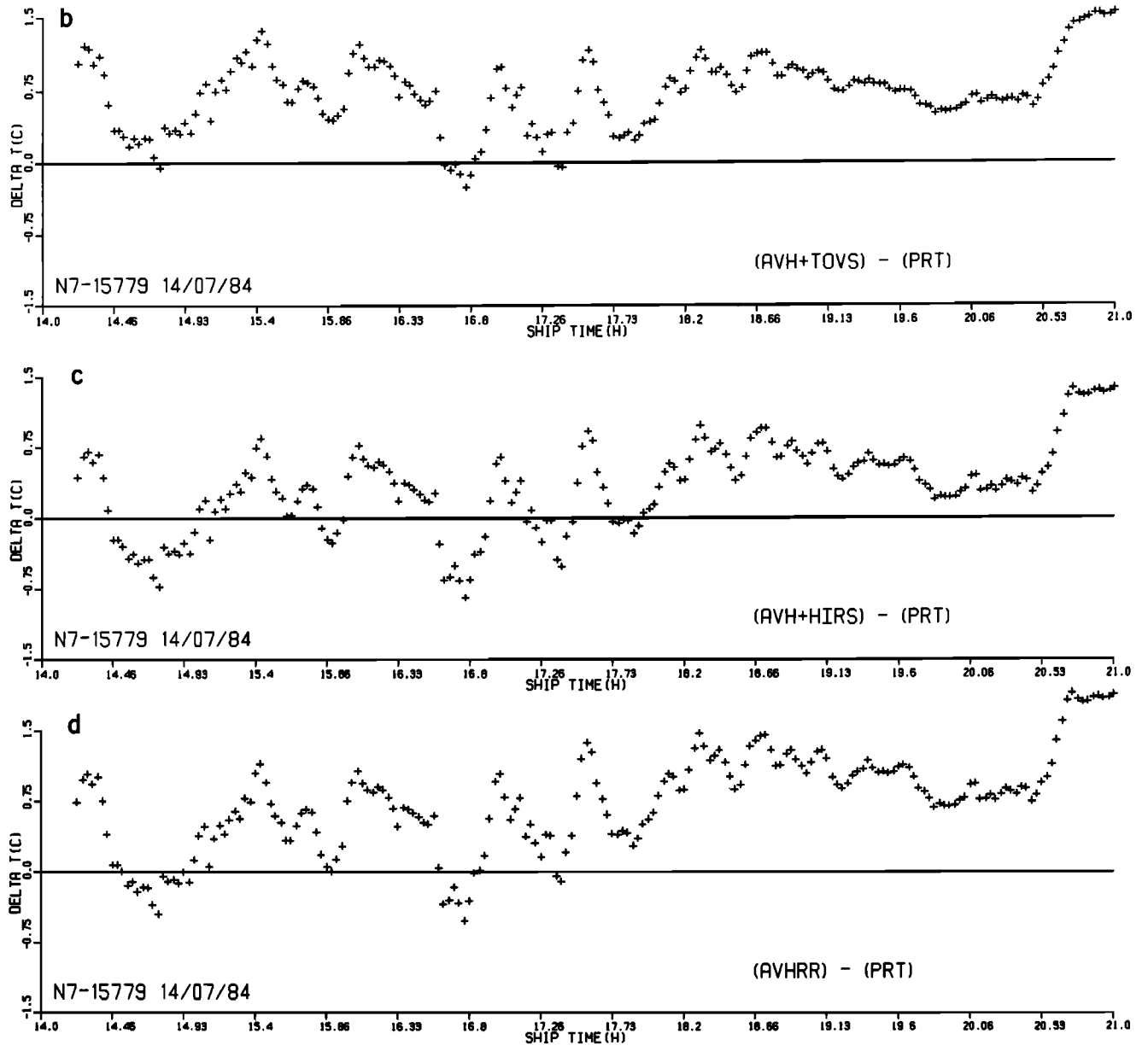

Fig. 8. (continued) Differences between PRT5 measured skin temperatures and (*b*) AVHRR plus TOVS retrieved skin temperatures, (*c*) AVHRR plus HIRS retrieved skin temperatures, and (*d*) AVHRR-only retrieved skin temperatures.

5. Comparison and Discussion of the Case Studies

For each of the above described NOAA 7 passes, a comparison has been performed by applying the different SST retrieval methods to the same satellite data with a subsequent computation of differences with ship measurements. The assumption was made that the sea surface temperature was constant during the day used for the comparison between ship track SSTs and the single satellite pass. Since comparisons are performed on a single-pixel basis, the retrieval coefficients including atmospheric and radiometric noise have been used. While all of the satellite measurements were done at scan angles between 35° and 45°, those coefficients for 40° seem adequate for this study. The first situation examined (orbit 17667, November 25, 1984) was characterized by fields of broken clouds, making simultaneous viewing of all the ocean's surface impossible. In addition, the sounder data (TOVS) are not usable, since all fields of view are cloud contaminated, demonstrating the limitation of using sounder data in this application. The cloud contamination is clearly shown by the tropospheric differences in temperature and dew point between TOVS and radiosonde atmospheric profiles (Figure 5*a*). The time series of the shipboard skin temperature (Figure 6*a*) on that day ranges between 12° to 14.5°C and shows some distinct SST frontal features. The deviation of the split window (scan angle dependent) SST estimates from the PRT5 measurements are given in Figure 6*b* (top of graph), together with a line (bottom of graph) indicating those measurements that are cloud contaminated (as defined by a cloud discrimination algorithm using the AVHRR visible channel 1 and the infrared channel 5; cloud contaminations are signified by flat maxima in the bottom graph of Figure 6*b*). Despite the limitations by clouds, the AVHRR-only method works quite well in the clear areas, as shown by the statistics in Table 5. A water vapor content of 1.7 g/cm^2 was measured by radiosondes launched from the ship, and the effect due to water vapor is properly corrected by the split window technique.

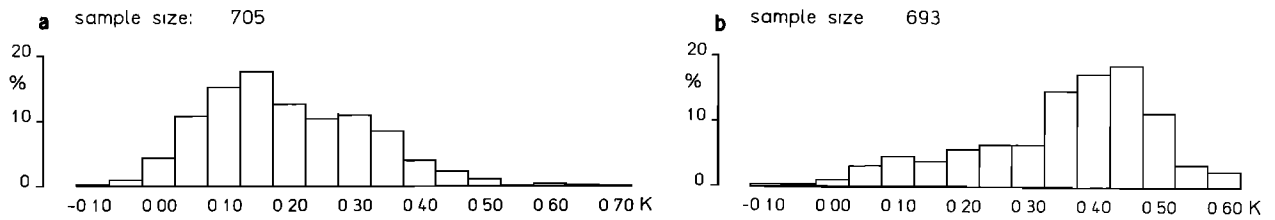

Fig. 9. Histograms of differences between bulk water temperature at a depth of 4 m and SST for (*a*) November 25 and (*b*) November 26.

The next comparison (orbit 17681, November 26, 1984) demonstrates very well the capability of the AVHRR plus HIRS combination to correct for extreme atmospheric situations. Figure 7*a* shows in situ skin temperatures along with the temperatures derived from the AVHRR using all three methods. The plot reveals that some pixels are cloud contaminated but were not rejected by the cloud pixel screening process. Colocated radiosondes, launched from R/V *Meteor* four times that day, give a total atmospheric water vapor amount of less than 0.9 g/cm^2. Here the AVHRR-only SST computation overestimates the atmospheric water vapor impact, leading to a strong positive bias in satellite-ship SST matchups. This bias is significantly reduced by applying the AVHRR plus HIRS formula to it. The temperature and dew point comparison between TOVS retrievals and the coincident (14 min apart) RAOB over the Atlantic is given in Figure 5*b*. The comparison shows that the TOVS performed very well over the dry winter atmosphere, giving 1.92°C temperature and 2.38°C dew point rms differences below the 300-mbar pressure level. This is an improvement over what earlier studies found [*Moyer et al.*, 1978; *Philips et al.*, 1979; *Hayden et al.*, 1981]. With the TOVS retrieved profiles, atmospheric transmission coefficients were calculated for AVHRR channels 4 and 5. Equation (1) was then used to calculate the surface temperature, and a correction was made for the emittance effect. Comparison between the corrected SST and the in situ skin temperatures shows a negative bias of −0.39°K and a standard deviation of 0.24°K. This result is better than the AVHRR-only method and differs only by 0.07°K from the AVHRR plus HIRS method when the rms values are compared. The total precipitable water measured by TOVS was 0.91 g/cm^2, compared with 0.86 g/cm^2 measured from the RAOB. The temperature deviations from the PRT5 temperature for all three methods are shown in Figures 7*b*–7*d*.

The third comparison uses data from the northeast Pacific Ocean. An examination of the in situ skin data for this day shows the cruise transect passing through a distinct frontal zone apparent in the infrared satellite image as colder (lighter colored) coastal water. Again, the AVHRR-alone SST calculation gives reasonable retrievals only when explicit use of the scan angle dependency is included. It still shows a rather large bias of 0.73°C caused by "abnormal" atmospheric conditions masking the ocean-emitted radiation. From the nearby RAOB data the atmosphere over the study area was characterized by warm, moist air below the 950-mbar level and convective instability at about 900 mbars. Addition of HIRS data again improves both the bias (now 0.33°C) and the rms differences compared with the in situ data (Figure 8*c*). The results of the TOVS method were less encouraging. The rms temperature and dew point differences were 2.6°C and 7.29°C, respectively, when compared with the RAOB data (Figure 5*c*). As is reported by *Hayden et al.* [1981], the most transparent HIRS water vapor channel (channel 10), which should have its peak at about 900 mbars, peaks instead at higher elevations, especially over the warm and moist surface region. This is precisely what happened during the moisture profile retrieval. HIRS water vapor channels, not being able to sense near the surface and having weighting functions much too wide to detect abrupt changes, resulted in overestimating the moisture content above the surface during the iterative process. The precipitable water content was estimated to be as much as twice the amount measured by the RAOB data (1.69 g/cm^2 and 0.89 g/cm^2, respectively). The bias and standard deviation of the AVHRR plus TOVS SST were 0.71°C and 0.36°C, respectively. This result is much worse than that with the AVHRR plus HIRS method but better than using AVHRR data alone.

In this context it is interesting to have a look at bulk-skin temperature differences for all 3 days considered. The comparison clarifies the atmospheric impact on the skin temperature. The first day (Figure 9*a*) shows only small differences between bulk and skin temperatures, with a mean of 0.15°C due to strong downwelling long-wave radiative flux from

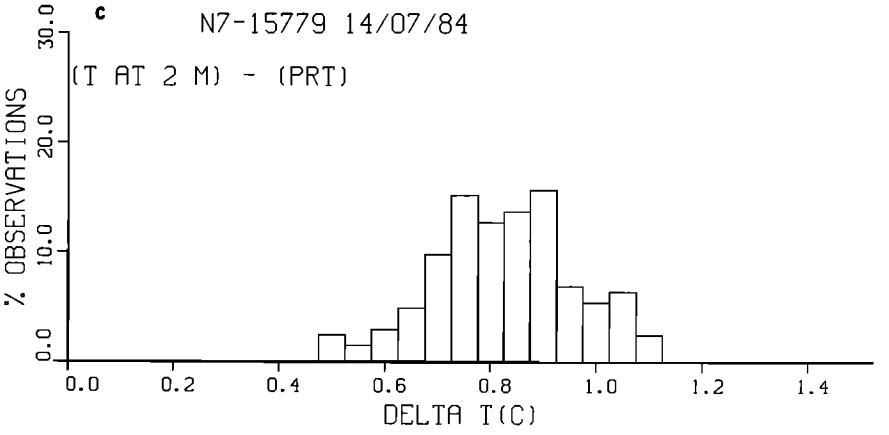

Fig. 9*c*. Histograms of differences between bulk water temperature at a depth of 2 m and SST for July 14.

clouds and water vapor emission. The clear sky of the second day (Figure 9*b*) leads to a prominent cooling of the surface skin, which then has a mean of 0.45°C. The third day comparison shows even larger bulk-skin temperature differences with a mean difference of 0.8°C (Figure 9*c*). The large differences are the result of a lack of vertical mixing and a strong surface cooling due to evaporation.

In a summary of our comparisons, the rms errors found lie well within the errors given by the retrieval formula and the radiometric noise in ship and satellite measurements. The biases are due to systematic atmospheric effects requiring more sophisticated analysis. The errors induced by atmospheric water vapor and temperature structures need to be corrected for in the SST algorithms, which should also account for scan angle dependence and nonblackbody ocean surface radiation. Remaining error sources are clouds not detected by the appropriate tests (e.g., subpixel clouds or thin cirrus clouds) and the extinction by atmospheric aerosol components when they differ from standard marine conditions [*Haenel*, 1976]. Both subpixel clouds and aerosol particles are able to modify the SST retrievals in a systematic way up to several tenths of a degree, as computed by radiative transfer simulations of the radiometer channels.

Another possible error source is the uncertainty in the pixel/ship colocations. Obviously, single fields of view are intersected by the ship's course on different secants, so that the 5-min ship tracks may fall partly out of the pixel selected. However, the error induced by this aspect should not be very large since the surface temperature seldom shows gradients of 0.5°C per pixel. The temporal variability of the ocean surface is not easy to quantify. It depends strongly on skin-bulk temperature differences, their destruction by wind-induced white caps, the diurnal heating of the surface layer, and dynamical processes like semidiurnal tides [*Robinson et al.*, 1984]. Nevertheless, the selected 1-day periods seem adequate to match up the ship and satellite measurements.

6. CONCLUSIONS

Computation of the AVHRR-only estimates from NOAA 7 data have rms accuracies of 0.9°C on a single-pixel basis if scan angle dependency is explicitly considered. Comparison with in situ skin measurements indicate strongly biased (up to 0.73°C) AVHRR SST estimates due to atmospheric structure effects. The addition of HIRS reliably decreases these biases (to approximately 0.3°C) caused by extreme atmospheric water vapor and temperature structures, as indicated by numerical modeling, and demonstrated by the comparison with in situ measured SST skin temperatures. The physical TOVS method, although very attractive, did not perform as well as the AVHRR plus HIRS method, especially under warmer, moist atmospheric conditions. This is expected, as TOVSs poorer performance is very closely linked with the poor vertical resolution of the HIRS water vapor channels. Thus improvements in the sensors and more sophisticated retrieval procedures may make the method very useful in many parts of the ocean.

A weakness of the SST retrieval methods considered here is their lack of proper detective schemes for cold thin clouds shifting satellite-measured temperatures to lower values. For the TOVS sounder, with its coarse spatial resolution, clouds are the limiting factor, since no declouding procedures are used to produce clear fields of view where there are partly cloud-contaminated spots. Generally, HIRS FOVs are too large to investigate mesoscale features even in fields of broken clouds. Contrary to this, significant improvement is possible for clear areas with the AVHRR/HIRS combination.

Acknowledgments. We would like to acknowledge the assistance of the crews of the R/V *Meteor* and M/V *Pandora II* in the collection of the in situ data. This study was supported by the German Research Agency, the Canadian Natural Science and Engineering Research Council, and the British Columbia Science Council. This support is gratefully acknowledged. A visit to Vancouver by the first author was supported by the Federal Republic of Germany (FRG) as part of a cooperative agreement between FRG and Canada. We are also grateful to H. Woolf of NOAA/NESDIS, Cooperative Institute for Meteorological Satellite Studies at the University of Wisconsin, for providing the TOVS export package. The cooperation of the Canadian Atmospheric Environment Service is also appreciated for supplying the RAOB data for the northeast Pacific region.

REFERENCES

Anding, D., and R. Kauth, Estimation of sea-surface temperature from space, *Remote Sens. Environ.*, *1*(4), 217–220, 1970.

Aoki, T., Statistical determination of clear radiance from cloud-contaminated radiances, *J. Meteorol. Soc. Jpn.*, *58*(6), 528–536, 1980.

Barton, I. J., Transmission model and ground-truth investigation of satellite-derived sea surface temperatures, *J. Clim. Appl. Meteorol.*, *24*, 508–516, 1985.

Bernstein, R. L., and D. B. Chelton, Large-scale sea surface temperature variability from satellite and shipboard measurements, *J. Geophys. Res.*, *90*, 11,619–11,630, 1985.

Brower, R. L., H. S. Gohrband, W. G. Pichel, T. L. Signore, and C. C. Walton, Satellite derived sea surface temperatures from NOAA spacecraft, *NOAA Tech. Memo. NESS 78*, 1–74, 1976.

Bruce, R. E., L. D. Duncan, and J. H. Pierluissi, Experimental study of the relationship between radiosonde temperatures and satellite-derived temperatures, *Mon. Weather Rev.*, *105*, 493–496, 1977.

Chahine, M. T., A general relaxation method for inverse solution of the full radiative transfer equation, *J. Atmos. Sci.*, *29*, 29–32, 1972.

Chahine, M. T., Generalization of the relaxation method for the inverse solution of nonlinear and linear transfer equations, in *Inversion Methods in Atmospheric Remote Sounding*, edited by A. Deepak, 622 pp., Academic, Orlando, Fla., 1977.

Clauss, E., H. Hinzpeter, and J. Mueller-Glewe, Messungen zur Temperaturstruktur im Wasser an der grenzflaeche Ozean-Atmosphere, *Meteor Forschungsergeb. Reihe B*, *5*, 90–94, 1970.

Dalu, G., Emittance effect of the remotely sensed sea surface temperature, *Int. J. Remote Sens.*, *6*(5), 733–740, 1985.

Dalu, G., C. Prabhakara, and R. C. Lo, Improved accuracy of the remote sensing of sea surface temperature, in *Oceanography from Space*, edited by J. Gower, pp. 109–114, Plenum, New York, 1981.

Deschamps, P. Y., and Y. Phulpin, Atmosphere correction of infrared measurements of sea surface temperature using channels at 3.7, 11 and 12 μm, *Boundary Layer Meteorol.*, *18*, 131–143, 1983.

Grassl, H., The dependence of the measured cool skin of the ocean on wind stress and total heat flux, *Boundary Layer Meteorol.*, *10*, 465–474, 1976.

Grassl, H., Gemessene Strahlungs- und Waermefluesse ueber dem Ozean, *Meteor Forschungsergeb. Reihe B*, *5*, 42–50, 1977.

Grassl, H., and H. Hinzpeter, The cool skin of the ocean, *GATE Rep. 14*, vol. I, pp. 229–236, World Meteorol. Org., Geneva, 1975.

Haenel, G., The properties of atmospheric aerosol particles as function of the relative humidity at the thermodynamic equilibrium with the surrounding air, *Adv. Geophys.*, *18*, 73–188, 1976.

Hasse, L., The sea surface temperature deviation and the heat flow at the sea-air interface, *Boundary Layer Meteorol.*, *1*, 368–379, 1971.

Hayden, C. M., W. L. Smith, and H. M. Woolf, Determination of moisture from NOAA polar orbiting satellite sounding radiances, *J. Appl. Meteorol.*, *20*, 450–466, 1981.

Hillger, D. W., Spatial and temporal variations in mesoscale water vapor retrieved from TOVS infrared radiances in a nocturnal inversion situation, *J. Clim. Appl. Meteorol.*, *23*, 704–723, 1984.

Hillger, D. W., and T. H. Vonder Haar, An analysis of satellite infrared soundings at the mesoscale using statistical structure and correlation functions, *J. Atmos. Sci.*, *36*, 287–305, 1979.

Kelly, G. A., B. W. Forgan, P. E. Powers, J. F. LeMarshall, M. Hassett, and B. O'Connor, A satellite-based operational system for

upper air analysis in the Australian region, *Remote Sens. Environ.*, *13*, 369–390, 1983.

Kelly, K. A., and R. E. Davis, An analysis of errors in sea surface temperature in a series of infrared images from NOAA 6, *J. Geophys. Res.*, *91*, 2633–2644, 1986.

Llewellyn Jones, D. T., P. J. Minett, R. W. Saunders, and A. M. Zavody, Satellite multichannel infrared measurements of sea surface temperature of the northeast Atlantic Ocean using AVHRR/Z, *Q. J. R. Meteorol. Soc.*, *110*, 613–631, 1984.

Maul, G. A., Zenith angle effects in multichannel infrared sea surface remote sensing, *Remote Sens. Environ.*, *13*, 439–451, 1983.

McAlister, E. D., and W. McLeish, Heat transfer in the top millimeter of the ocean, *J. Geophys. Res.*, *74*, 3408–3414, 1969.

McClain, E. P., Multiple atmospheric-window techniques for satellite-derived sea surface temperatures, in *Oceanography from Space*, edited by J. Gower, pp. 73–85, Plenum, New York, 1981.

McClain, E. P., W. G. Pichel, C. C. Walton, Z. Ahmad, and J. Sutton, Multi-channel improvements to satellite-derived global sea surface temperatures, *Adv. Space Res.*, *2*(6), 43–47, 1983.

McClain, E. P., W. G. Pichel, and C. C. Walton, Comparative performance of AVHRR-based multichannel sea surface temperatures, *J. Geophys. Res.*, *90*, 11,587–11,601, 1985.

McMillin, L. M., Estimation of sea surface temperature from two infrared window measurements with different absorption, *J. Geophys. Res.*, *80*(36), 5113–5117, 1975.

McMillin, L. M., and D. S. Crosby, Theory and validation of the multiple window sea surface temperature technique, *J. Geophys. Res.*, *89*(C3), 3655–3661, 1984.

Moyer, V., J. R. Scoggins, N. M. Chou, and G. S. Wilson, Atmospheric structure deduced from routine Nimbus-6 satellite data, *Mon. Weather Rev.*, *106*, 1340–1352, 1978.

Olesen, F. S., and H. Grassl, Cloud detection and classification over oceans at night with NOAA-7, *Int. J. Remote Sens.*, *6*, 1435–1444, 1985.

Paulson, C. A., and J. J. Simpson, The temperature difference across the cool skin of the ocean, *J. Geophys. Res.*, *86*, 11,044–11,054, 1981.

Philips, N., L. M. McMillin, A. Gruber, and D. Wark, An evaluation of early operational temperature soundings from TIROS-N, *Bull. Am. Meteorol. Soc.*, *60*(10), 1188–1197, 1979.

Prabhakara, C., G. Dalu, and V. G. Kunde, Estimation of sea surface temperature from remote sensing in the 11- to 13-micron window region, *J. Geophys. Res.*, *79*(33), 5039–5044, 1974.

Robinson, I. S., N. C. Wells, and H. Charnock, The sea surface thermal boundary layer and its relevance to the measurement of sea surface temperature by airborne and spaceborne radiometers, *Int. J. Remote Sens.*, *5*(1), 19–45, 1984.

Saunders, P. M., Shadowing on the ocean and the existence of the horizon, *J. Geophys. Res.*, *72*(18), 4643–4649, 1967.

Saunders, R. W., An automated scheme for the removal of cloud contamination from AVHRR radiances over western Europe, *Int. J. Remote Sens.*, *7*, 3–27, 1985.

Smith, W. L., H. M. Woolf, C. M. Hayden, A. J. Schreiner, and J. M. LeMarshall, The physical retrieval TOVS export package, paper presented at First International TOVS Study Conference, Igls, Austria, 1983.

Strong, A. E., Drifting buoys used to maintain accuracy, *Trop. Ocean Atmos. Newsl.*, *25*, 1984.

Strong, A. E., and E. P. McClain, Improved ocean surface temperatures from space—Comparisons with drifting buoys, *Bull. Am. Meteorol. Soc.*, *65*, 138–142, 1984.

Ulivieri, C., Minimization of atmospheric water vapor and surface emittance effects on remotely sensed sea surface temperature, *IEEE Trans. Geosci. Remote Sens.*, *GE-22*(6), 622–626, 1984.

Weinreb, M. P., H. E. Fleming, L. M. McMillin, and A. C. Neuendorffer, Transmittance for the TIROS Operational Vertical Sounder, *NOAA Tech. Rep. NESS 85*, 1–60, 1981.

W. J. Emery and H.-Y. Shin, Department of Oceanography, University of British Columbia, Vancouver, British Columbia, Canada V6T 1W5.

H. Grassl, Forschungszentrum Geesthacht, Max Planck Strasse, 2054 Geesthacht, Federal Republic of Germany.

P. Schluessel, Institut für Meereskunde, Düsternbrooker Weg 20, 2300 Kiel, Federal Republic of Germany.

(Received March 24, 1986;
accepted June 19, 1986.)